Interaction of $NaYF_4$:Er:Yb Nanoparticles with Phospholipid Monolayers as Models of Biological Membranes

LIVIA PETRESCU[1*], OTILIA CINTEZA[2], ANA-MARIA VOICULESCU[3], TUDOR ROSU[2], IONUT ENCULESCU[4], ELENA MATEI[4], SERBAN GEORGESCU[3], RUXANDRA BIRJEGA[3], SPERANTA AVRAM[1], DAN MIHAILESCU[1]

[1]University of Bucharest, Faculty of Biology, 91-95 Splaiul Independenţei, Bucharest, Romania.

[2]University of Bucharest, Faculty of Chemistry, 21 Dumbrava Rosie, 020462, Bucharest, Romania

[3] National Institute for Laser, Plasma and Radiation Physics, 409 Atomiştilor Street, Măgurele, Ilfov, Romania

[4] National Institute for Materials Physics, 105 bis Atomiştilor Str, Măgurele, Ilfov, Romania

Given the evolution of imaging techniques in the biomedical field is becoming more necessary to develop sensitive markers, less toxic and not least more economical. Upconverting luminescent nanocrystals doped with rare earth ions, excited in infrared and emitting in visible, are considered real concurrent to classical fluorescent markers, featuring a number of advantages in rapport with them. The aim of this study is to prepare $NaYF_4$ nanoparticles doped with erbium and ytterbium for biological applications in bioimaging techniques. After synthesis, upconverting nanoparticles were coated with SiO_2 for surface sealing and passivation. The nanoparticles were characterized by X-ray diffraction, luminescence spectroscopy, electronic microscopy and dynamic light scattering. The interaction of the nanoparticles with mimicking cell membrane models was studied. $NaYF_4$ nanoparticles showed a good size distribution and good emission efficiency. The uncoated nanoparticles increase the fluidity of the lipid monolayer, while the effect of the silica coated nanoparticles is substantially reduced.

Keywords: up-conversion; $NaYF_4$; biomarkers, biocompatibility; cell membrane models

Luminescent particles have attracted great interest in various scientific areas: electronics (light-emitting diodes – LED), displays, solar cells, lasers, street lighting and paint industry [1-5]. Upconversion luminescent nanoparticles (oxides and fluorides doped with rare earth ions)have brought new perspectives in bioanalytical science, especially in imaging techniques.

The upconverting nanoparticles, excited in infrared (IR) with emission in visible, present a series of advantages in rapport with 'classical' fluorescent markers: improved signal-to-noise ratio, increased tissue penetration, reduced photo-bleaching, reduced photo-toxicity and low price cost [6, 7].

One of the best candidates for upconversion is Er^{+3} whose energy level scheme present many energy resonances. The most efficient transitions in visible are $(^4S_{3/2}, {}^2H_{11/2}) \rightarrow {}^4I_{15/2}$ (in green) and ${}^4F_{9/2} \rightarrow {}^4I_{15/2}$ (in red). For IR pump, a suitable pump transition is ${}^4I_{15/2} \rightarrow {}^4I_{11/2}$ (at ~ 0.98 μm), where efficient and not expensive laser diodes exist. Erbium being a rare earth, its absorption lines are narrow and less intense. Increasing the erbium concentration to improve the absorption of pump radiation leads to the onset of cross-relaxation processes as $((^4S_{3/2}, {}^2H_{11/2}) + {}^4I_{15/2}) \rightarrow ({}^4I_{9/2} + {}^4I_{13/2})$ which depopulates the emitting levels non-raditively, thus reducing the emission efficiency.

The solution was given by Auzel [8-10], by codoping with Yb^{3+}. Yb^{3+} has intense and broad absorption band at 980 nm, its very simple energy level scheme (only two energy levels, ${}^2F_{7/2}$ and ${}^2F_{5/2}$) precludes upconversion losses. The Yb^{3+} transition ${}^2F_{5/2} \rightarrow {}^2F_{7/2}$ is resonant with Er^{3+} transitions ${}^4I_{15/2} \rightarrow {}^4I_{11/2}$ and ${}^4I_{11/2} \rightarrow {}^4F_{7/2}$; from ${}^4F_{7/2}$, via rapid multiphonon transitions, excitation reaches the emitting levels. Therefore, the erbium concentration is keeping low (few percents) and the ytterbium concentration is quite large (10 – 20%).

The synthesis of upconversion fluorescent inorganic nanoparticles suitable as bio-probe remains a major challenge. The size of targeted molecules (for example, proteins, oligo-nucleotides and other biomolecules in cells or tissues) ranges from several to tens nanometers. For applications in biological field, the size of the luminescent particles should be in the nanometer domain and with a narrow size distribution, with high emission efficiency and and water dispersible [11]. Besides, they should be resistant to photobleaching, biocompatible, and non-toxic. Till now, hexagonal $NaYF_4$ doped with erbium and ytterbium proved to be one of the most efficient upconverting material.

This article reports on the synthesis and characterization of $NaYF_4$:Er^{3+}:Yb^{3+} nanoparticles and their coating with a passivating layer to increase the biocompatibility for cells. In order to apply these nanoparticles to biological structures, we studied the interaction of the nanoparticles with phosphatidylcholine monolayers that mimic the cell membrane.

Experimental procedures

Synthesis of $NaYF_4$ nanoparticles doped with rare-earth ions

In our studies the $NaYF_4$:Er:Yb nanoparticles were synthesized using a hydrothermal method 12]. We tested different chelating agents (Ethylene-diaminetetraacetic acid, citric acid and sodium citrate) and molar ratios between components (Y/Yb/Er=88:10:2, Y/Yb/Er=80:19:1, Y/Yb/Er=80:18,5:1,5). Optimal formula was chosen based on size distribution and conversion efficiency [13].

The materials used were $Y(NO_3)_3 \cdot 6(H_2O)$, $Yb(NO_3)_3 \cdot 5(H_2O)$, $Er(NO_3) \cdot 5(H_2O)$ and NaF (purchased from Sigma-Aldrich). The chelating agent was EDTA (Ethylene-diaminetetraacetic acid).

The molar ratio of the metals was Y/Yb/Er = 80:18.5:1.5. To the mixture of aqueous solutions of $Y(NO_3)_3 \cdot 6(H_2O)$,

* email: draghicilivia@yahoo.com; Tel: 0722520816

$Yb(NO_3)_3 \cdot 6(H_2O)$ and $Er(NO_3)_3 \cdot 5(H_2O)$ was added an aqueous solution of chelating agent. Under a vigorous stirring, a white complex was obtained. Then, an aqueous solution of NaF was added and stirred again for an hour. The new formed complex was transferred to a teflon lined stainless steel autoclave. The autoclave was heated with 0.2°C/min up to 155°C, maintained at 155°C for 48 hours and then cooled with 0.08°C/min. The obtained $NaYF_4:Yb^{3+}:Er^{3+}$ precipitate was separated by centrifugation (Heraeus-Christ GMBH centrifuge, 2000 rpm, 20 min), washed for several times with deionized water and centrifuged again in the same conditions. After drying at 40°C (forced convection oven Venticell 5S) the $NaYF_4:Yb^{3+}:Er^{3+}$ crystallites were obtained.

Characterization of the obtained $NaYF_4$:Er:Yb nanoparticles

The obtained nanoparticles were characterized using X-ray diffraction (XRD), electron microscopy, dynamic light scattering (DSL) and optical spectroscopy (diffuse reflectance and upconversion luminescence spectra). The X-ray diffraction measurements were performed on a PAnalytical X'Pert PRO MPD diffractometer (CuKα). The $NaYF_4$:Er:Yb nanoparticles were analyzed with the scanning electron microscope Zeiss Evo 50 with a LaB6 cathode in the high vacuum mode, assuring a 2 nm resolution. To achieve high-resolution observations of morphology of samples, these were covered with a thin layer of Cu, about 20 nm thick (DC sputering). Besides the morphology, with a 133 eV energy resolution, the elemental composition of the samples was determined (EDX analysis). The size and size distribution of the particles were measured by using dynamic light scattering (DLS) instrument Nanozeta sizer ZS (Malvern Instruments Ltd.) in the range of 0.6nm - 6μm. All DLS diagrams were collected in the scattering intensity, number and volume modes, with water or alcohol as dispersant media. The samples were diluted with distilled water (1:25) and dispersed by ultrasonication (~ 5 min) prior to the measurement. For coated nanoparticles the surface potential was also determined, on the same instrument, using 0.1 M KCl solution as dilution medium.

The luminescence of the $NaYF_4$:Er:Yb nanoparticles was excited in IR at 980 nm with laser diode DioPower JOLD-30-CPXF-1L. The luminescence spectra were measured using a Horiba Jobin-Yvon 1000M monochromator, an S-20 photomultiplier and an SR830 lockin amplifier. The experimental setup for diffuse reflectance measurements was described elsewhere [14].

Coating $NaYF_4$:Er:Yb nanoparticles for biocompatibilization

The up-converting nanoparticles as prepared were subject to an encapsulation procedure using silica as biocompatible material. The nano-encapsulation was performed using a modified Ströber method [15].

Briefly, 3 mg of nanoparticles were suspended in 7 mL ethanol, and 0.85 mL deionized water and 0.25 mL concentated ammonia. Separately the silane derivatives were prepared as follows: 10 μL APTES (3-aminopropyl) trietoxysilane dissolved in 0.5 mL ethanol and 10 μL TEOS (tetraethyl orthosilicate) dissolved in 1 mL ethanol. The $NaYF_4$:Yb:Er nanoparticles were stirred with magnetic stirrer for one hour, while TEOS solution was added dropwise. The hydrolisis of silane derivative was performed for 4 h in order to allow the formation of silica shell. For further functionalization of the surface, APTES solution was added at the end of the synthesis.

Characterization of coated nanoparticles

To determine the coating effect on the structure and morphology of nanoparticles, they are analyzed by scanning electron microscopy. The elemental composition of the samples was determined with the EDX analysis module.

Size, size distribution and surface charge of coated nanoparticles were investigated using dynamic light scattering (DLS) method, as described above.

Preparation of PC Langmuir monolayer and $NaYF_4$:Er:Yb nanocrystals and measurement of pressure–area isotherm.

In this work were studied the interactions between $NaYF_4$: Er:Yb nanocrystals (coated and uncoated) and the phosphatidylcholine (PC) in Langmuir monolayers, serving as model membranes [16-18].

An autorecording KVS NIMA Langmuir deposition trough (total area=98 cm^2) was used to record compression isotherms of monolayers of PC and $NaYF_4$ spread onto the aqueous subphase. (Phosphatidylcholine was purchased from Avanti Polar Lipids). The spreading solutions were prepared by dissolving the investigated compounds weighed to an accuracy of 0.01 mg, in ethanol. Spreading solutions were deposited onto the water subphase with a Hamilton microsyringe (accuracy 2.0 μL). After spreading, the monolayers were left to equilibrate for 15 min before the compression was initiated with a barrier speed of 20 cm^2/min.

The interaction with $NaYF_4$ nanoparticles was studied by injected a nanoparticle dispersion under the monolayer (in the aqueous subphase) and let the system to equilibrate (30 min).

All experiments were run at 22 ± 1°C and the results are averaged values on at least three measurements. The experimental uncertainty was estimated to be 0.2 mN/m.

Isotherms analysis

In order to verify the influence of $NaYF_4$:Yb:Er nanocrystals on the state of phospholipids monolayers, the compression modulus values (C_s^{-1}) for all of the investigated mixed systems were calculated from the π-*A* isotherms according to eq. (1).

$$C_s^{-1} = -A\frac{d\pi}{dA} \quad (1)$$

where π is the surface pressure and *A* is the specific surface of the lipid molecule in the water/air interface.

The C_s^{-1}-π relationships provide information on the physical state of a monolayer [19, 20]. C_s^{-1} values below 12.5 mN/m would account for the gaseous state, those in the range of 13-50 mN/m for the liquid-expanded state, those from 100 up to 250 mN/m, for the liquid condensed state, and those above 250 mN/m, for the solid state of the monolayer [21, 22].

Results and discussions

Electron microscopy characterization

The image of the $NaYF_4$:Yb:Er nanoparticles, obtained with the scanning electron microscope, is given in figure 1. The chelating agent is EDTA and the molar ratio of the metals is Y:Yb:Er = 80:18.5:1.5. This molar ratio lead to optimal sizes and shapes for biomedical applications. The shape of the particles is close to spherical; the size distribution is narrow, the average size being approximately 70 nm.

The elemental composition of the particles (EDX analysis) is shown in figure 2.

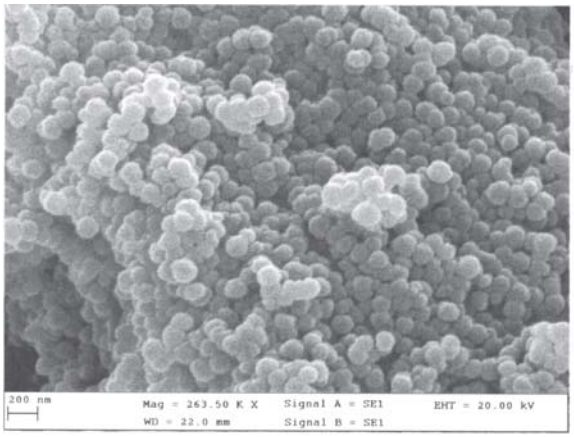

Fig. 1. Electron microscope image of the $NaYF_4$:Er:Yb nanoparticles synthesized with the molar metal ratio Y:Yb:Er = 80:18.5:1.5. The size distribution is narrow, the average size is ~ 70 nm

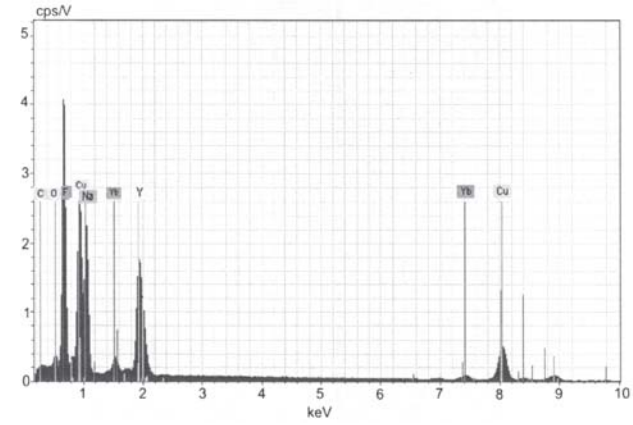

Spectrum: Acquisition

El	AN	Series	unn. C [wt.-%]	norm. C [wt.-%]	Atom. C [at.-%]	Error [%]
C	6	K-series	3.05	2.81	6.89	0.4
O	8	K-series	3.78	3.49	6.42	0.5
F	9	K-series	32.45	29.95	46.37	3.7
Na	11	K-series	20.06	18.51	23.69	1.4
Cu	29	K-series	19.68	18.16	8.41	0.6
Y	39	L-series	24.43	22.55	7.46	1.0
Yb	70	L-series	4.91	4.53	0.77	0.2
		Total:	108.35	100.00	100.00	

(a)

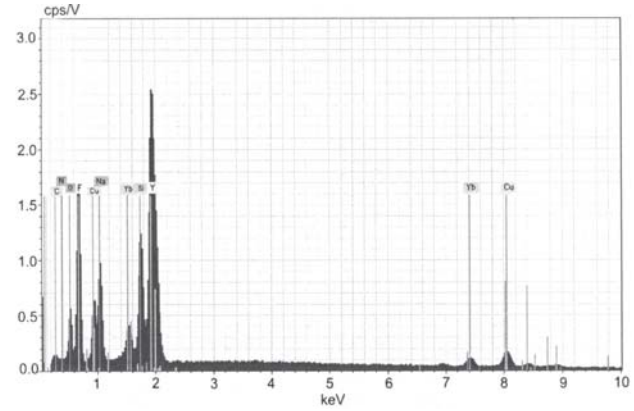

Spectrum: Acquisition

El	AN	Series	unn. C [wt.-%]	norm. C [wt.-%]	Atom. C [at.-%]	Error [%]
C	6	K-series	1.83	1.99	4.73	0.3
N	7	K-series	6.03	6.59	13.40	1.2
O	8	K-series	6.30	6.89	12.26	0.9
F	9	K-series	25.61	27.98	41.94	3.2
Na	11	K-series	6.44	7.04	8.72	0.5
Si	14	K-series	4.26	4.65	4.72	0.2
Cu	29	K-series	4.61	5.03	2.26	0.2
Y	39	L-series	31.90	34.85	11.16	1.4
Yb	70	L-series	4.55	4.97	0.82	0.2
		Total:	91.54	100.00	100.00	

(b)

Fig. 2. Results of EDX analysis. (a) $NaYF_4$:Yb:Er nanoparticles; b) silica coated $NaYF_4$:Yb:Er nanoparticles

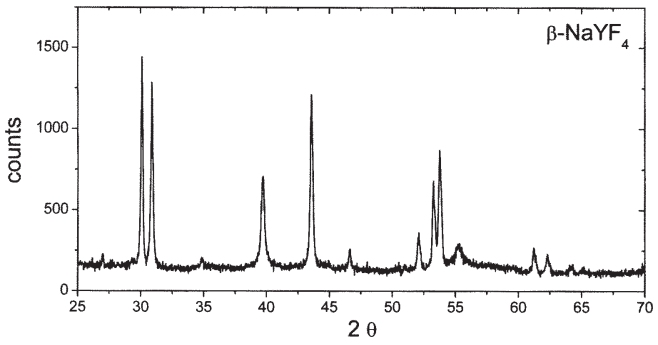

Fig. 3. XRD pattern of the $NaYF_4$:Er:Yb powder. The diffraction lines correspond to the hexagonal phase β-$NaYF_4$

The EDX spectra prove the existence of the $NaYF_4$ matrix. Due to the very small amount of Er codopant, erbium is not shown in the EDX spectra. Silica is present in the EDX spectrum of the coated nanoparticles.

XRD

The XRD pattern of the $NaYF_4$:Yb:Er powder is shown in figure 3. Only the diffraction lines corresponding to β-$NaYF_4$ (hexagonal phase, Card PDF 00-016-0334) are present.

The average size (coherence domain) determined with the Scherrer relation is ~ 70 nm, in agreement with the electron microscope data. Therefore, the $NaYF_4$:Yb:Er particles are single phases.

DLS characterization and Zeta potential

The size and size distribution of the nanoparticles were also evidenced in the DLS measurements (fig. 4).

As it is expected, the size of the nanoparticles is increasing after the deposition of the silica shell. The sample remain monodisperse, no separate phases of silica nanoparticles without up-converting nanoparticles are obtained.

The surface potential was in agreement with the presumable surface characteristics from the synthesis: + 5.8 mV for EDTA stabilized nanoparticles, - 10 mV for silica coated and + 18 mV for APTES modified silica coated nanoparticles (the values are the average of 20 data obtained from zeta potential, measured on Nanozeta sizer ZS, as it is described in the previous section). The surface potential values obtained for silica coated nanocrystals are in good agreement with the composition of silica shell.

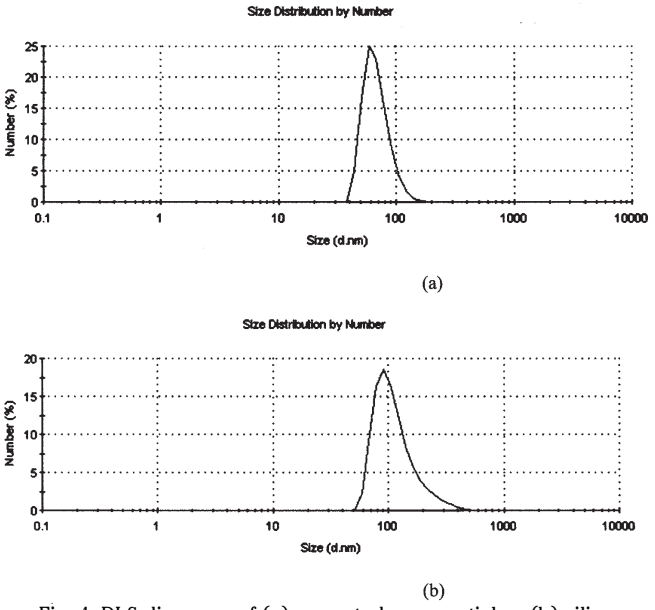

Fig. 4. DLS diagrams of (a) uncoated nanoparticles; (b) silica encapsulated nanoparticles

Thus, when TEOS is used as silane precursor, the surface of the silica shell contains –OH groups, while when APTES is used some $–NH_2$ groups are located onto the surface, leading to the modification of the surface potential to a positive value.

Langmuir monolayer study

The interfacial behavior of nanoparticle suspensions, obtained after complete removal of the solvent used for their synthesis, was analyzed at the air/water interface and in the presence of phosphatidylcholine lipid monolayers mimking a biomembrane (fig. 5).

The presence of the uncoated $NaYF_4$:Yb:Er nanoparticles stabilized with EDTA leads to an expanded monolayer, as it is shown in a shift of the isotherm. In table 1, are summarized the results of the computation of compression modulus for the PC monolayer in the presence of $NaYF_4$:Yb:Er particles.

The computation of the compression modulus proves the increase of the value of these characteristics, thus the increase in the fluidity of the lipid monolayer. The influence of the uncoated nanoparticles is more evident than those of the silica coated particles.

The state equation proposed by Birdi [23]

$$(\Pi + \Pi_{CO})(A - A_0) = kT \quad (2)$$

Table 1
THE COMPRESSION MODULUS OF LIPID MONOLAYER IN THE PRESENCE OF VARIOUS CONCENTRATIONS OF UP-CONVERTING NANOPARTICLES

Sample	Nanoparticles concentration	C
Uncoated NP	0	
	50	33.2
	100	33.8
	300	31.0
Coated NP	0	
	50	16.3
	100	21.8
	300	32.5

is used to describe the liquid expanded state of the lipid monlayer, where A_0 is the minimum specific surface of the lipid molecule in the deposited monolayer (at the maximum packaging state) and Π_{CO} is a correction factor dealing with the cohesion energy in the monolayer. In the table 2 are shown the cohesion factors for the PC monolayers with and without uncoated nanoparticles in the subphase.

The values of the cohesion correction terms are decreasing with the increase of the uncoated nanoparticles in the subphase, supporting the conclusion that the lipid monlayer became more expanded under the influence of the up-converting $NaYF_4$:Yb:Er nanoparticles.

Diffuse reflectance

The diffuse reflectance spectrum of the $NaYF_4$:Yb:Er powder in rapport with the 'white' $BaSO_4$ is given in figure 6. In the 920 – 1000 nm wavelength domain, the absorption lines of Yb^{3+} (transition $^2F_{7/2} \rightarrow {}^2F_{5/2}$) and Er^{3+} (transition $^4I_{15/2} \rightarrow {}^4I_{11/2}$) are superposed, i.e. these transitions are resonant, assuring a good energy transfer between Yb^{3+} and Er^{3+}.

We observe the intense absorption peak at ~ 975 nm due to the absorption of Yb^{3+}.

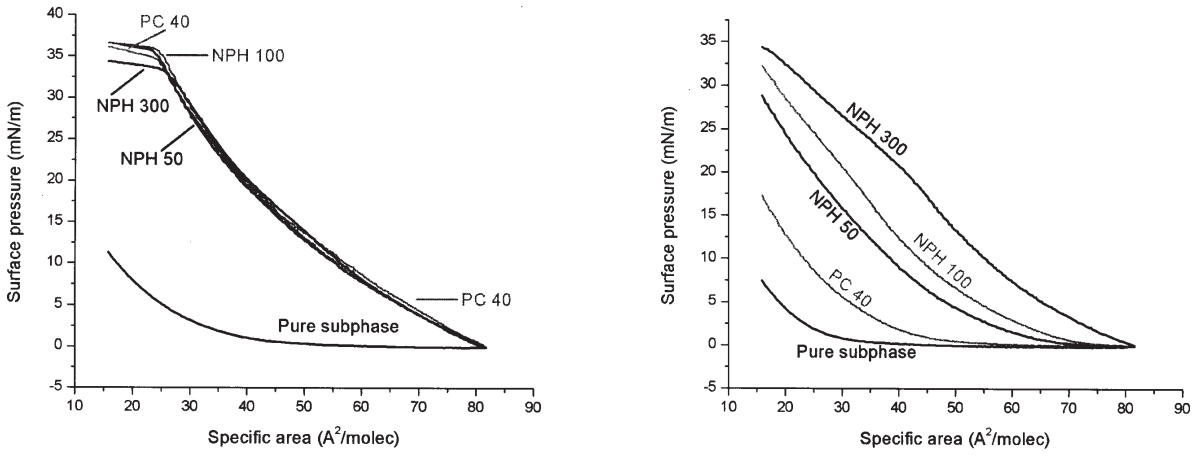

Fig. 5. The surface pressure isotherm of PC with various concentration of up-converting nanoparticles in the subphase (a) uncoated nanoparticles; (b) silica encapsulated nanoparticles

Table 2
COHESION BIRDI FACTOR FOR THE PC MONOLAYERS IN THE PRESENCE OF UNCOATED $NaYF_4$:Yb:Er NANOPARTICLES

	Π_{CO}		
Molecular specific surface (A2/molecule)	NP added in the subphases (micorliters)		
	0	50	100
100	1.89	1.74	0.72
95	3.36	3.24	1.91
90	4.96	4.75	3.27

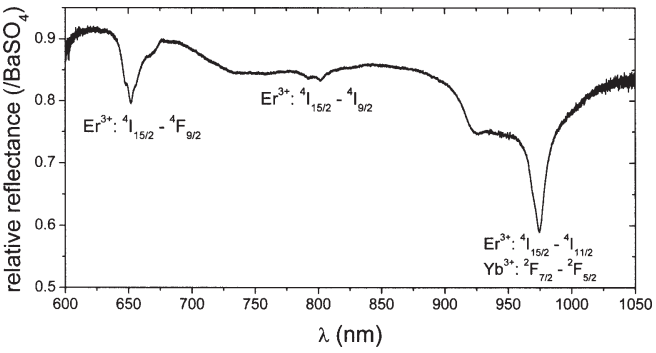

Fig.6. Diffuse reflectance spectrum of $NaYF_4$:Yb:Er powder in rapport with the 'white' $BaSO_4$.

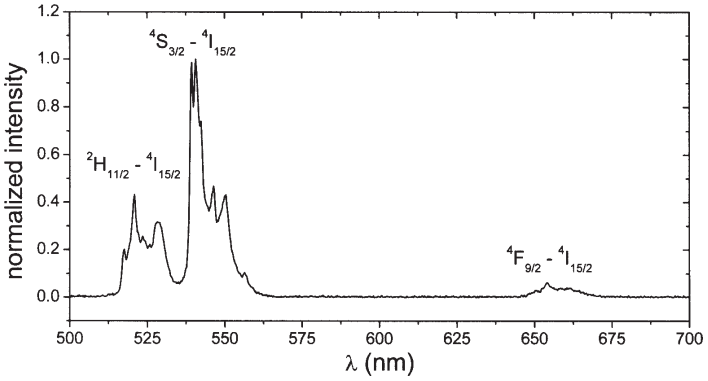

Fig. 7. Luminescence spectrum of Er^{3+} in $NaYF_4$:Yb:Er excited in IR, at 980 nm. The spectrum is not corrected for the spectral sensitivity of the experimental apparatus.

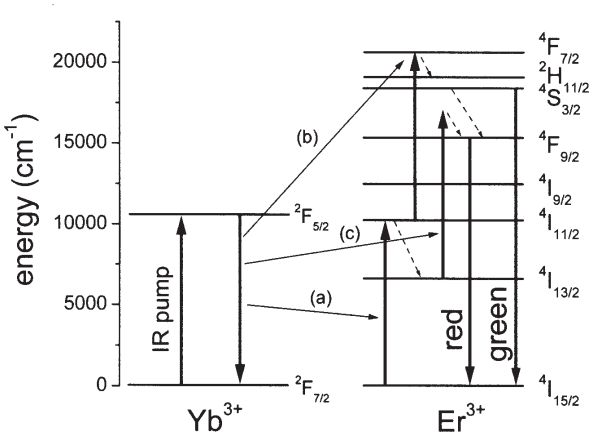

Fig. 8. Energy level scheme of Yb^{3+} and Er^{3+} in $NaYF_4$ and the main processes leading to the population of the emitting Er^{3+} levels.

Luminescence spectrum

The luminescence spectrum of Er^{3+} in NaYF4:Yb:Er excited in IR at 980 nm is given in figure 7. The emission lines are $(^2H_{11/2}, {}^4S_{3/2}) \rightarrow {}^4I_{15/2}$ (green luminescence) and ${}^4F_{9/2} \rightarrow {}^4I_{15/2}$ (red luminescence). The above parenthesis symbolizes the thermalisation of Er^{3+} levels $^2H_{11/2}$ and $^4S_{3/2}$ at room temperature.

The main processes responsible for the upconversion luminescence are sketched in figure 8.

For pumping at 980 nm, the light is absorbed by both Er^{3+} and Yb^{3+} ions, but the absorption of Er^{3+} is very week in rapport with those of Yb^{3+}. Therefore, in the following we can consider that only ytterbium ions absorb. In figure 7 are shown three Yb-Er energy transfer processes: (a) $^2F_{5/2}$ (Yb^{3+}), $^4I_{15/2}$ $(Er^{3+}) \rightarrow {}^2F_{7/2}$ (Yb^{3+}), $^4I_{11/2}$ (Er^{3+}); as the result of the process (a), the level $^4I_{11/2}$ (Er^{3+}) is populated. The level $^4I_{11/2}$ (Er^{3+}) being populated, the process (b) becomes possible: $^2F_{5/2}$ (Yb^{3+}), $^4I_{11/2}$ $(Er^{3+}) \rightarrow {}^2F_{7/2}$ (Yb^{3+}), $^4F_{7/2}$ (Er^{3+}); from $^4F_{7/2}$ (Er^{3+}), via multiphonon transitions, the green emitting Er^{3+} levels $^4S_{3/2}$ and $^2H2_{11/2}$ are populated. Via multiphon and (weak) radiative processes from $^4S_{3/2}$, the red emitting level $^4F_{9/2}$ is populated. Besides, there is another Yb3+ - Er3+ process which contribute to the population of $^4F_{9/2}$: (c) $^4F_{5/2}$ (Yb^{3+}), $^4I_{13/2}$ $(Er^{3+}) \rightarrow {}^2F_{7/2}$ (Yb^{3+}), $^4F_{9/2}$ (Er^{3+}). This process is not resonant and involves emission of phonons. The long lifetime level $^4I_{13/2}$ (Er^{3+}) is populated by multiphonon transitions from $^4I_{11/2}$ (Er^{3+}). Due to the long lifetime, this level can accumulate a significant population. Therefore, even if the process (c) is a phonon-assisted one, it may have a contribution to the population of $^4F_{9/2}$ (Er^{3+}).

In figure 9 is shown an image of the luminescence of a suspension of $NaYF_4$:Yb:Er particles in water excited in IR (at ~980 nm). The dominant emsion is green,

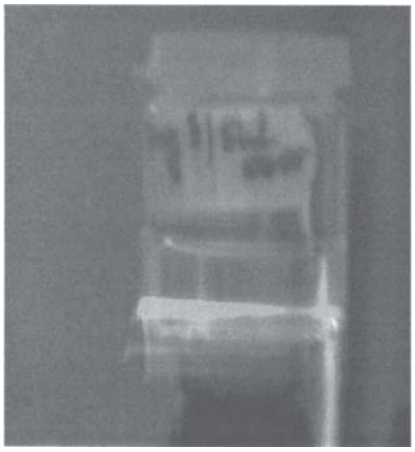

Fig. 9. Upconversion luminescence of a $NaYF_4$:Yb:Er suspension excited at ~980 nm

Conclusions

$NaYF_4$ nanoparticles co-doped with rare-earth ions were synthesized using a hydrothermal method in various conditions. We aimed to obtain optimal nanoparticle as size and shape for application to biological samples. Optimal metal molar ratio was found to be Y:Yb:Er =

80:18.5:1.5. $NaYF_4$ nanoparticles showed a good size distribution and good emission efficiency. The second aim of this research was to increase the nanoparticles biocompatibility by coating with SiO_2. The interaction of the nanoparticles with mimicking cell membrane models was studied. The uncoated nanoparticles increase the fluidity of the lipid monolayer, while the effect of the silica coated nanoparticles is substantially reduced.

In conclusion, it was demonstrated that $NaYF_4$ nanoparticles doped with erbium and ytterbium coated with silica are good candidates for biomedical applications.

Future work will involve studies of cell viability in presence of $NaYF_4$ nanoparticles as well as specific antibody binding for immunofluorescence techniques.

Acknowledgement: This work was supported by the Romanian National Center for Management of Programs (CNMP), PNCDII/project 62060/2008 and PNCDII/project 12135/2008.

References

1. WANG, F., HUANG, X. H., WANG, H. B., LIU, J. P., FAN, Y. M., ZHU, Y. Z., JIN, Z., Spectros. Spectral Analysis, 31, 2011, p. 1446.
2. ZHAO, H., LIU, G., ZHANG, J., POPLAWSKY, J. D., DIEROLF, V., TANSU, N., Opt. Express, **19**, 2011, p. A991.
3. ZHANG, J., LI, Q., DI, X., LIU, Z., XU, G., Nanotechnology, **19**, 43, 2008, p. 435606
4. SHAN, G. B., ASSAAOUDI, H., DEMOPOULOS, G. P., ACS Appl. Mater. Interfaces, **3**, 2011, p. 3239
5. DONG, Y., XU, J., ZHOU, G., ZHAO, G., JIE, M., YANG, L., SU, L., QIU, J., FENG, W., LIN, L., Opt Express, **14**, 5, 2006, p. 1899
6. HEER, S., KÖMPE, K., GÜDEL, H.-U., HAASE, M., Advanced Mater. **16**, 2004, p. 2102.
7. JALIL, R. A., Y. ZHANG, R. A., Biomaterials, **29**, 2008, p. 4122
8. AUZEL, F. C. R. Acad. Sc., Paris Ser. B, **262**, 1966, p. 1016.
9. AUZEL, F. C. R. Acad. Sc., Paris Ser. B, **263**, 1966, p. 765.
10. AUZEL, F., Chem. Rev. **104**, 2004, p. 139.
11. STOUWDAM, J. W., F.. VAN VEGGEL, C. J. M., Nano Letters, **2**, 2002, p. 733.
12. SUN, Y., CHEN, Y., TIAN, L., Yu, Y., KONG, X., ZHAO, J., ZHANG, H, Nanotehnology, **18**, 2007, p 275609
13. COTOI, E., VOICULESCU, A.M., GEORGESCU, S., TOMA, O., ROSU, T., BRAN, L., BORCA, E., J. Optoelectron. Adv. Mater.- Symposia, **1**, 2009, p. 689.
14. GEORGESCU, S., VOICULESCU, A. M., TOMA, O., TISEANU, C., GHEORGHE, L., ACHIM, A., MATEI, C., Optoelectron. Adv. Mater. – Rapid Commun. **3**, nr. 12, 2009, p. 1379
15. STRÖBER, W., FINK, A., BOHN E.; J. Colloid Interface Sci., **26**, 1968, p. 62.
16. MAGET-DANA, R., Biochim Biophys Acta, **1462**, 1-2, 1999, p. 109.
17. BREZESINSKI, G., MOHWALD, H., Adv Colloid Interface Sci, **100-102**, 2003, p. 563-84
18. CADENHEAD, D. A., MULLER-LANDAU, F., Can. J. Biochem. Cell Biol., **62**, 1984, p. 732.
19. DAVIES, J. T.; RIDEAL, E. K. Interfacial Phenomena, 2nd ed.;Academic Press: New York, 1963; p 265.
20. HARKINS, W. D. The Physical Chemistry of Surface Films; Reinhold Publishing Co.: New York, 1954; p 107.
21. AMBIKE, A., ROSILIO, V., STELLA, B., LEP TRE-MOUELHI, S., COUVREUR, P., Langmuir, **27**, 2011, p. 4891.
22. HAC-WYDRO, K., KAPUSTA, J., JAGODA, A., WYDRO, P. and DYNAROWICZ-LATKA, P., Chem Phys Lipids, **150**, 2, 2007, p. 125.
23. BIRDI, K. S., MADSEN, F., EBERTH, K, Colloid. Polym. Sci., **272**, 1994, p. 1000.

Manuscript received: 6.12.2011